Composites Science and Technology 251 (2024) 110583

Contents lists available at ScienceDirect

Composites Science and Technology

journal homepage: www.elsevier.com/locate/compscitech

One-pot strategy for the preparation of nanoparticles grafted with bimodal polymers: An *in-silico* insight

Jinyuan Mao [a,b], Jiajia Zhou [a,b,*], Hong Liu [c,**]

[a] South China Advanced Institute for Soft Matter Science and Technology, School of Emergent Soft Matter, South China University of Technology, Guangzhou, 510640, China

[b] Guangdong Provincial Key Laboratory of Functional and Intelligent Hybrid Materials and Devices, South China University of Technology, Guangzhou, 510640, China

[c] Key Laboratory of Theoretical Chemistry of Environment Ministry of Education, School of Environment, South China Normal University, Guangzhou, 510640, China

ARTICLE INFO

Keywords:
Nanocomposites
Bimodal polymer
Grafting-to & grafting-from
One-pot strategy
Computer simulation

ABSTRACT

Polymer nanocomposites composed of polymer-grafted nanoparticles (NPs) have garnered significant interest due to their diverse functional applications in various domains. The emerging concept of bimodal polymer brushes within the grafting-nanoparticle framework offers control over interfacial entropic and enthalpic interactions. Here, we introduce a novel one-pot strategy that integrates "grafting-to" and "grafting-from" methods to create polymer-grafted bimodal NPs. Utilizing coarse-grained molecular dynamics simulations with a stochastic reaction model, we explore the factors influencing grafting density and polydispersity in these NPs. Our findings demonstrate that this one-pot strategy achieves a polydispersity similar to the two-step "grafting-from then grafting-to" process, while attaining a moderate grafting density comparable to the "grafting-to then grafting-from" approach. Consequently, we analyze factors such as "grafting-from" reaction rates, and initial feeding ratios, step-addition techniques which collectively influence the final grafting density and polydispersity index within this one-pot strategy. This comprehensive investigation enhances our understanding of the kinetics behind synthesizing bimodal polymer-grafted NPs and offers insights for designing polymer-based nanocomposites with improved performance.

1. Introduction

Polymer nanocomposites, characterized by a blend of polymer matrices as the predominant element and nanoparticles (NPs) as the minor component, have garnered substantial interest due to their wide range of technological and industrial applications, including biocompatibility, colloidal stabilization, sensors, and electromagnetic materials, etc. [1–4]. In recent decades, polymer nanocomposites incorporating polymer-grafted NPs, often referred to as "hairy" NPs, have captivated the attention of both computational and experimental researchers [5–7]. The blending of NPs not only contributes to improved material properties, but also significantly broadens the scope of potential applications. The initial incorporation of inorganic nanoparticles into hydrophobic polymer matrices faced difficulties due to strong segregation of NPs. Approaches involving monomodal brushes were employed to manipulate the miscibility of grown/ligand chains by covalently grafting them onto NP surfaces [8]. However, it is important to note that monomodal brush-grafted NPs tend to aggregate due to the delicate balance between entropic and enthalpic interfacial interactions, and the dispersion state depends on factors such as NP concentration and size, polymer chain molecular weight, and grafting approach [9,10].

Nowadays, inorganic silica NPs [11–13], Clay [14], Graphene Oxide (GO) [15], Multi-Walled Carbon Nanotube (MWCNT) [16] and gold NPs [17–19] grafted with polymer brushes have been extensively investigated for their ability to enhance the functional performance of polymer nanocomposites by controlling the dispersion of NPs within polymer matrices [20]. In addition, it can also be grafted with polymers to direct their self-assembly into unique architectures in bulk and at interfaces [21,22]. Careful design of grafted polymer polydispersity holds promise for enhancing NP dispersion. Recent years have witnessed a surge in scientific inquiries focusing on the influence

* Corresponding author at: South China Advanced Institute for Soft Matter Science and Technology, School of Emergent Soft Matter, South China University of Technology, Guangzhou, 510640, China.

** Corresponding author at: Key Laboratory of Theoretical Chemistry of Environment Ministry of Education, School of Environment, South China Normal University, Guangzhou, 510640, China.

E-mail addresses: zhouj2@scut.edu.cn (J. Zhou), hongliu@m.scnu.edu.cn (H. Liu).

https://doi.org/10.1016/j.compscitech.2024.110583
Received 5 February 2024; Received in revised form 20 March 2024; Accepted 1 April 2024
Available online 4 April 2024

of polydispersity in the stabilization of NPs within nanocomposites [23–26]. For instance, a judicious design of long and short grafted chains can lead to reduced interparticle attraction and consequently promote well-dispersed nanocomposites. Additionally, considerable attention has been dedicated to achieve high grafting densities of NPs, which can promote complex self-assembled nanostructures [9,27].

A category of polymer-grafted NPs is termed "bimodal" (or bidispersed), defined by grafted chains possessing two distinct monodisperse lengths [28]. These polymer-grafted NPs exhibit superior dispersion and controlled interactions within polymer matrices in comparison to the previously mentioned monomodal polymer-grafted NPs [29]. Previous studies have outlined methods to synthesize these bimodal polymer-grafted NPs. For instance, Minko et al. devised a combined "grafting-to" and "grafting-from" approach to create bimodal brushes on plate surfaces [30]. Rungta and colleagues outlined a versatile step-by-step strategy by employing reversible addition-fragmentation chain transfer (RAFT) polymerization, enabling independent control over grafting density, molecular weight, composition, etc. [29]. Cheng et al. presented a novel strategy, merging "grafting-to" and "grafting-from" techniques, to assemble gold NPs with isotropic surface chemistry into anisotropic plasmonic dimers with high yield. They initially attached polyethylene glycol (PEG) and an atom transfer radical polymerization (ATRP) initiator onto 40 nm gold NPs through "grafting-to", followed by poly (methyl methacrylate) (PMMA) "grafting-from" growth. The results demonstrated uniform dispersion of PEG- and PMMA-modified gold nanospheres in the favorable solvent N, N-dimethylformamide (DMF) [19]. Chen et al. also introduced a tandem "grafting-to" and "grafting-from" method for producing amphiphilic gold nanocrystals coated with amphiphilic diblock polymer brushes [17]. This approach offers a robust means to fine-tune filler dispersion at the NP interface, paving the way for novel nanocomposite material development. However, due to experimental limitations, *in-situ* observation of the grafting reaction process remains challenging, hindering an exploration of grafted-polymer conformation from a microscopic perspective. Numerical simulation studies, particularly coarse-grained molecular simulations (CGMD), can not only elucidate the intricacies of the grafting reaction process *in-situ*, but also offer efficiency and cost-effectiveness compared to experimental methods.

In this study, we focus on nanoparticles (NPs) anchored with bimodal polymer chains, a configuration achieved through a combination of grafting-to (GT) and grafting-from (GF) strategies. We employ CGMD simulations with a stochastic reaction model [28]. Illustrated in Fig. 1, we have schematically demonstrated the implementation of three distinct schemes for various grafting reaction processes for bimodal polymer-grafted NPs. The first scheme employs a two-step process involving GT followed by GF, where ligand chains are initially grafted to the NPs, succeeded by the grafting of monomers from the nanoparticle interface (referred to as GT-GF). The second scheme reveres the steps (referred to as GF-GT), where monomers are first grafted from the nanoparticle interface, followed by the grafting of ligand chains to the NPs. Furthermore a one-pot scheme has also been formulated, encompassing simultaneous grafting to ligand chains and grafting from monomers (illustrated in Fig. 1 as GT&GF). Our simulations show that the one-pot GT&GF scheme exhibits precedence over the other two schemes, with regard to both grafting density and the polydispersity. Subsequently, we conduct an in-depth exploration of several factors, such as reaction rate of the "grafting from" process, initial feeding ratios, and stepwise addition operation. Our research aims to provide a clearer understanding of the kinetic processes involved in the fabrication of bimodal brush-anchored NPs through the one-pot GT&GF strategy. Moreover, the insights gained from our work are anticipated to offer valuable guidance for the well-informed design and enhancement of the functional performance of polymer-grafted nanocomposites.

2. Model and computational details

The construction of the NP was achieved through the icosahedral best covering method, based on the tables of spherical codes with icosahedral symmetry [31]. The incorporation of a hollow NP model was strategically chosen to substantially enhance computational efficiency, as a single-layer of covering spheres effectively prevents the infiltration of other particles into the NP's interior. As depicted in Fig. 2, eight NPs of identical size (with a diameter $D_{NP} = 10\sigma$) were arranged in a three-dimensional array with dimensions of 2 × 2 × 2, featuring 506 grafted initiator sites (type A) for the GT process and 126 grafted initiator sites (type B) for the GF process. These NPs were positioned within a cubic simulation box measuring 80σ in length. The initial configurations of monomers (type M) and ligand chains (T-C) were established by randomly placing 12 800 and 3840 within the simulation box, ensuring no overlaps. Here, we keep the ratio at ≈4:1 (3840 ligand chains with 13 monomer/chain to 12 800 monomers) with the initiator sites of A:B≈4:1. The distinct chemical species have not been addressed within the context of this paper.

We conducted Langevin molecular dynamics simulations, employing the rigid-body approach [32] for NPs, within an *NVT* ensemble. The simulations were executed utilizing the GALAMOST package [33]. Our simulation protocol commenced with the maintenance of a constant temperature and consistent time settings. The consistent time settings refers to the total reaction time in GT-GF and GF-GT being the same as in GT&GF. Specifically, we employed the LJ energy scale ε_{LJ}, alongside a temperature of $T^* = 1.0\ K_BT/\varepsilon_{LJ}$, and a time step of $dt = 0.001\ \sigma(m/\varepsilon_{LJ})^{1/2}$.

The non-bond interactions governing all pairs of beads were modeled under a purely repulsive regime, employing the standard LJ potential with truncation at 3.0σ:

$$U_{ij} = \begin{cases} 4\varepsilon_{ij}\left[\left(\frac{\sigma}{r_{ij}}\right)^{12} - \alpha\left(\frac{\sigma}{r_{ij}}\right)^{6}\right] & , r_{ij} < 3.0\sigma \\ 0 & , r_{ij} \geq 3.0\sigma \end{cases} \quad (1)$$

where $\alpha = 0.4$ corresponds to a "Θ solvent" condition [28,34,35]. We shift the standard LJ potential to be zero at $r_{ij} = 3\ \sigma$. In this context, we have defined simulation units by setting $m = 1$, $\sigma = 1$, and $\varepsilon = 1$ for simplicity.

The bonding between adjacent C–C and C–T beads, representing polymer connectivity, is modeled using the finitely extensible nonlinear elastic (FENE) potential. This potential is defined as follows:

$$U_{\text{polymer}} = -\frac{1}{2}kr_{\max}{}^2 \ln\left(1 - \frac{r^2}{r_{\max}^2}\right) \quad (2)$$

where $k = 30.0\,\varepsilon/\sigma^2$, and $r_{\max} = 1.5\,\sigma$ [36].

Initially, a preperiod simulation comprising $10^2\,\tau$ was executed to mitigate the impact of the initial configuration prior to the grafting reaction. Subsequently, a grafting reaction period was simulated to replicate the GT and GF reaction processes. To achieve bimodal polymer brushes, we formulated three distinct schemes: GT-GF, GF-GT, and GT&GF. In the GT-GF scheme, the grafting process was divided into two steps. Initially, the grafting of extended ligand chains was conducted for a duration of $5 \times 10^4\,\tau$, followed by the growth of shorter ligand chains via the reaction between monomers (M) and particle B of the NP, again spanning $5 \times 10^4\,\tau$. Similarly, the GF-GT process followed a comparable approach. Notably, the GT&GF scheme encompassed a one-pot process, sustained for $10^5\,\tau$. Further particulars can be found in Table 1. As a general practice, a set of three parallel samples was employed for each data point, and unless explicitly specified, error bars are presented in the figures throughout this article.

The grafting-reaction processes of GF and GT were executed using a stochastic reaction model, wherein the concept of reaction probability (P_r) was introduced to regulate the rate of grafting reactions. Further elaboration on this can be found in our previous works [37,38]. In

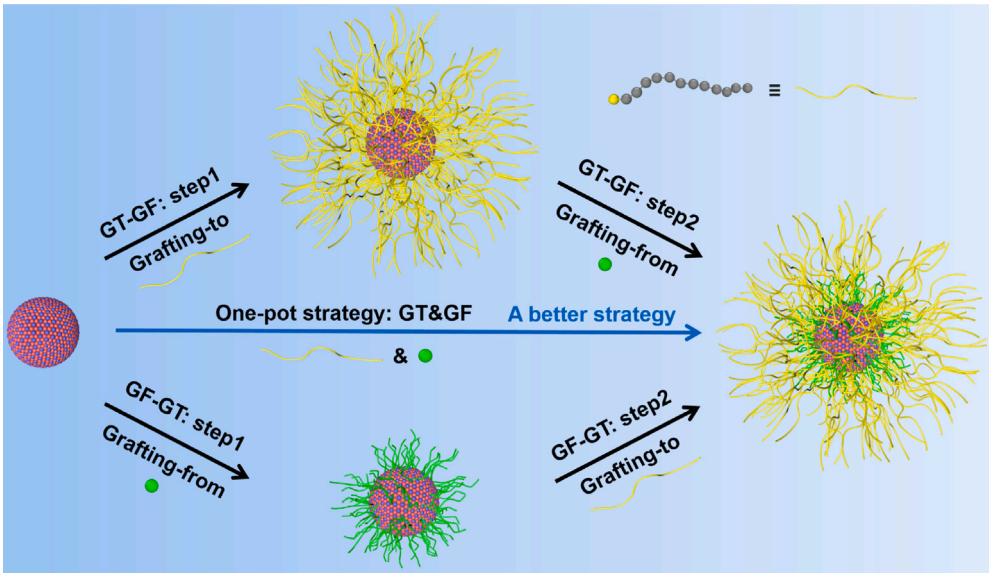

Fig. 1. Three schematic illustrations depict the grafting reaction process. The nanoparticle is depicted with 506 grafted initiator sites (red bead), capable of participating in the Grafting-to (GT) reaction process with the ligand chain (yellow chain). Additionally, 126 grafted initiator sites (blue bead) are present, facilitating the Grafting-from (GF) reaction process with the monomer (green bead).

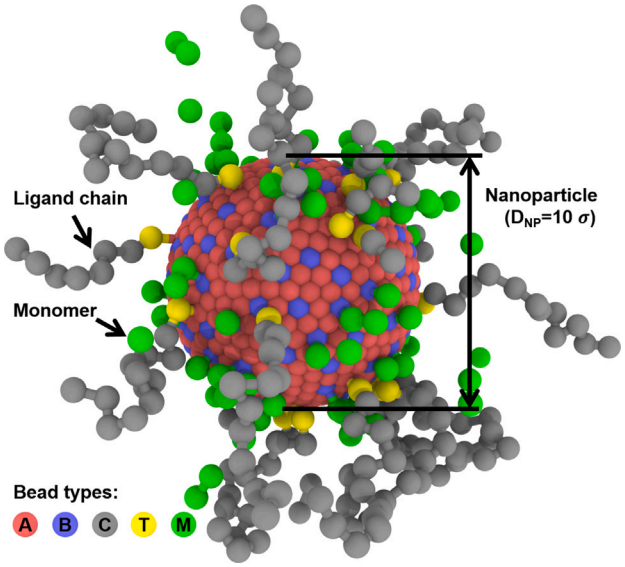

Fig. 2. The snapshot obtained from the simulation depicts the initial configurations of the nanoparticle, ligand chain, and monomer. The nanoparticle, possessing a diameter of $D_{NP} = 10\sigma$, is characterized by 506 grafted initiator sites (type A) capable of interacting with the ligand chain (T-C, comprised of 13 beads), as well as 126 grafted initiator sites (B) that facilitate interaction with the monomer (type M).

Table 1
The three different schemes for the preparation of bimodal polymer brushes onto NPs.

Scheme	Step1 (Time, τ)	Step2 (Time, τ)	P_r
GT-GF	5×10^4	5×10^4	$P_r(A-T) = 0.5$,
GF-GT	5×10^4	5×10^4	$P_r(B-M) = 1.0$,
GT&GF	10^5		$P_r(M-M) = 0.002$

essence, during specific time intervals within the GF reaction, several monomers (M) within a predetermined interaction radius approach the NP's surface (particle B). From this pool of monomers, one is chosen to participate in a reaction with the NP. The GT reaction follows a similar principle, wherein the ligand chain end of particle T reacts with NP of particle A. The decision as to whether a monomer connects with active monomers is based on a comparison between a generated random number and a predefined P_r. Post-reaction, the connected entities become the growth centers following the polymerization process as

$$A^* + T^*C\cdots CCC \rightarrow A - TC\cdots CCC \quad (3)$$

$$B^* + M^* \rightarrow B - M^* \quad (4)$$

$$B - M^* + M^* \rightarrow B - M - M^* \quad (5)$$

where $P_r(A-T) = 0.5$ is assigned for the GT reaction process, and $P_r(B-M) = 1.0$, $P_r(M-M) = 0.002$ for the GF reaction process. The consistent reaction interval period $\Delta t = 0.05\,\tau$ is maintained. These parameter settings effectively account for any negligible impact of transport constraints related to monomer diffusion to the reaction site [28].

3. Results

In our simulation setup, the NPs are permitted to move freely throughout the grafting reaction process. Consequently, we consider the distinct competitive effects arising from ligand chains and monomers due to entropic and enthalpic interfacial interactions, respectively. With this consideration, we have devised three distinct schemes (GT-GF, GF-GT, GT&GF) to execute the grafting reaction over a cumulative duration time of $10^5\,\tau$. Throughout this process, we have recorded the complete trajectory to capture the evolution of grafting density (η) and polydispersity index ($Đ$) of monomers. Here, the grafting density is defined as $\eta = n_{chain}/[4\pi(D_{NP}/2)^2]$, where n_{chain} signifies the number of ligand or grown chains (initiator sites grafted from monomers forming a chain) anchored to the NP's surface, and D_{NP} represents the NP's diameter.

As illustrated in Fig. 3a, both the GT&GF and GF-GT schemes attain a saturation grafting density of grown chains ($\eta_{grown} = 0.40$). The GT-GF scheme remains at an near-saturation state ($\eta_{grown} = 0.36$) within the allocated reaction time. It is conceivable that when the NP is extensively grafted with ligand chains, the monomers might encounter challenges in accessing the NP's surface freely. In the GT-GF scheme, the grafting density of ligand chains (Fig. 3b) reaches its highest point at $\eta_{ligand} = 0.27$, followed by GT&GF ($\eta_{ligand} = 0.10$), while the GF-GT scheme demonstrates an extremely low value of $\eta_{ligand} = 0.01$. These observations are further elucidated in Fig. 3c, where η_{total} is

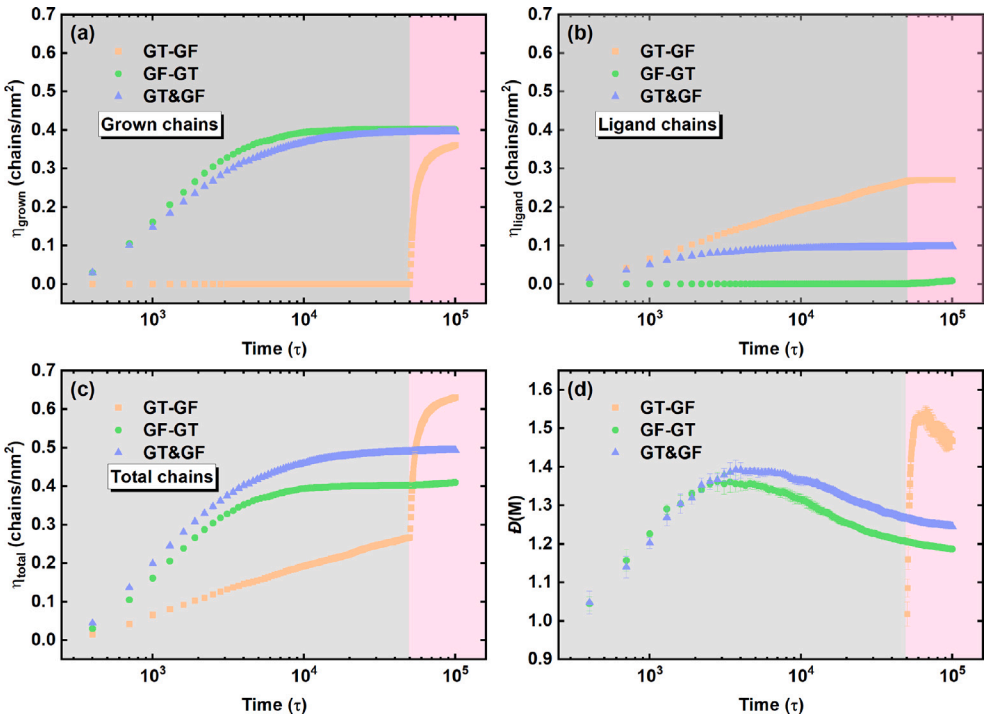

Fig. 3. The variations in (a) η_{grown}, (b) η_{ligand}, (c) η_{total}, and (d) $Đ$(M) are depicted concerning the progression of grafting-reaction time within three distinct schemes (GT-GF, GF-GT, GT&GF). The gray and pink regions distinguish the two-step processes.

plotted against reaction time. The analysis implies that achieving a well-balanced total grafting density within the GT&GF scheme, rather than employing both GF-GT and GT-GF strategies, shows potential for guiding the rational design of one-pot GT&GF nanocomposites due to their inherent convenience.

The variability of grown chains is of paramount concern to researchers, encapsulated by $Đ$(M). This index is defined as the ratio of weight-average molar mass to number-average molecular mass:

$$Đ(\mathrm{M}) = \frac{\bar{M}_w}{\bar{M}_n} = \frac{\sum_i N_i M_i^2 / \sum_i N_i M_i}{\sum_i N_i M_i / \sum_i N_i} \tag{6}$$

As depicted in Fig. 3d, the $Đ$ fluctuations observed in the GF-GT and GT&GF schemes, transitioning from a peak value of 1.40 to a final level of 1.25, signify these two strategies as more favorable choices under a sufficiently precise reaction duration. Although the dispersity index ($Đ$(M)) in GT&GF remains at 1.25, exceeding the typical values of approximately 1 observed in other surface living polymerization methods such as ATRP and RAFT, our focus remains on comparing the one-pot strategy to the two-step strategies (GF-GT and GT-GF), which inherently sacrifice some polydispersity. The GT-GF strategy holds the high value of $Đ$(M) $\approx$ 1.50 under the allocated reaction time. The lower value of $Đ$(M) observed in both the GF-GT and GT&GF schemes can be attributed to the early involvement of monomers in the reaction. In contrast, the GT-GF scheme initiates the GF reaction only after the GT process of ligand chains, hindering the exposure of monomers to the surface of NPs and thus leading to a higher $Đ$(M) in this scheme. Furthermore, the slightly elevated $Đ$(M) in the GF&GT scheme compared to GF-GT also implies that the GT process significantly influences the grafting of monomers in GF process. In conclusion, an alternative perspective highlights the profound impact of grafting order, whether it involves GF, GT, or a combination thereof, on the ensuing properties of the grafted target products (grown and ligand chains). Representative snapshots of the grafted nanoparticles obtained at different times within three distinct schemes (GT-GF, GF-GT, and GT&GF) can be found in Fig. 4.

We can not only control the chain length in our simulation but also estimate the chain length or even the mean-squared end-to-end distance

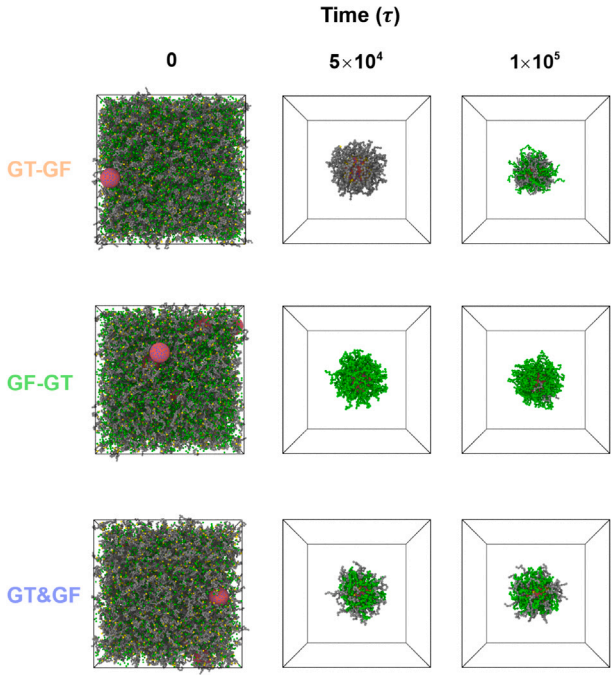

Fig. 4. Representative snapshots of the grafted nanoparticles obtained at different times within three distinct schemes (GT-GF, GF-GT, and GT&GF). For clarity, we show a single nanoparticle along with its grafted chain at times $5 \times 10^4\ \tau$ and $1 \times 10^5\ \tau$.

($\langle R_{ee}^2 \rangle$) of each chain. Here, we present the $\langle R_{ee}^2 \rangle$ of grafted grown and ligand chains as a function of reaction time (Fig. 5). Remarkably, in both of three schemes, the rate of change of $\langle R_{ee}^2 \rangle$ of grafted ligand chains have no significant divergence. while the grown chains attain a uniform value of $\langle R_{ee}^2 \rangle = 80$ within the GT&GF and GT-GF schemes. The grafted grown chains in GF-GT scheme keep at a plateau of $\langle R_{ee}^2 \rangle = 50$

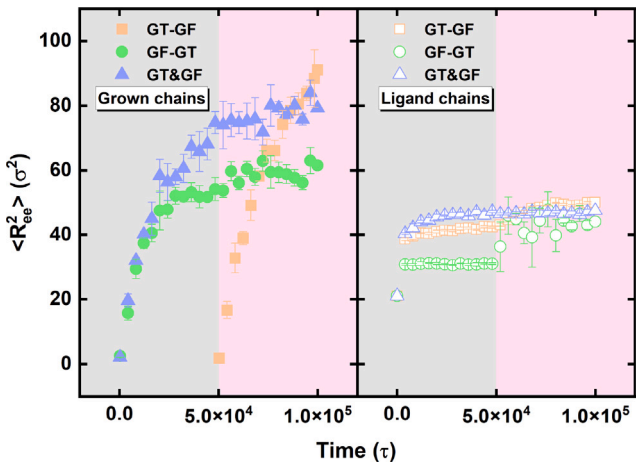

Fig. 5. The relationship between mean-square end-to-end distance ($\langle R_{ee}^2 \rangle$) of grafted grown and ligand chains and the progression of grafting-reaction time is illustrated across three different schemes (GT-GF, GF-GT, GT&GF). The gray and pink regions distinguish the two-step processes.

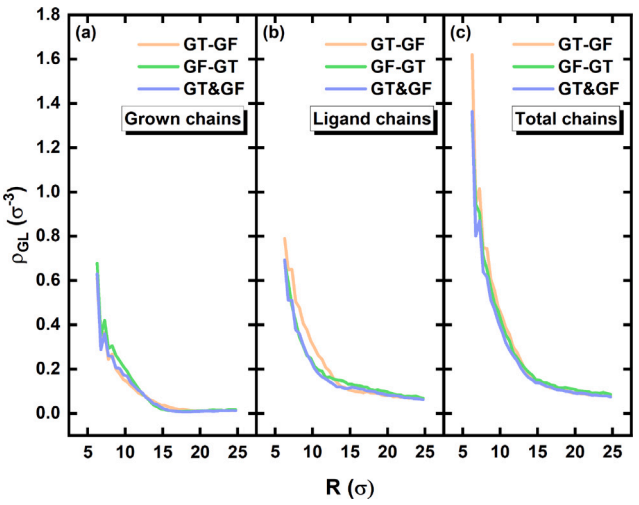

Fig. 6. The relationship between graft-layer density (ρ_{GL}) and distance from the distance of center of the nanoparticle (R) is elucidated for grafted grown chains, ligand chains, and the overall chain count, using a defined sliced thickness of $dR = 0.5\,\sigma$.

even in the first step of "grafting from" process (time $< 5 \times 10^4\,\tau$). This observation underscores the superiority of the one-pot GT&GF scheme, even when compared with the terminal reaction aspect of GF-GT scheme. These inherent advantages hold significant promise for enabling industrially controlled processes, facilitating the design of tailored materials with desired properties.

The graft-layer density (GLD) of a NP, which characterizes the grafting density surrounding the NP, is a pivotal focus within the nanocomposites domain [39]. In this context, the GLD is defined as $\rho_{GL} = N_{GL}/\{\frac{4\pi}{3}[(R + dR)^3 - R^3]\}$, where N_{GL} signifies the number of monomers (from either grown chains or ligand chains) within the grafted layer around the NP, $R = D_{NP}/2$ denotes the NP's radius, and $dR = 0.5\,\sigma$ represents the thickness of the sliced grafted layer. As illustrated in Fig. 6a, we have plotted the GLD against the distance within the sliced graft layer. Within the GF-GT scheme, the ρ_{GL} of grown chains achieves a maximum value (~0.68) at a distance of $6\,\sigma$ (the distance from the center of NP to the first monomer), closely followed by the GT&GF schemes (~0.63) and GT-GF (~0.61). The ρ_{GL} of ligand chains in GT-GF scheme demonstrates the highest ρ_{GL} value at 0.79 (Fig. 6b), while both the GT&GF and GF-GT schemes share an equivalent ρ_{GL} value of 0.69 at a distance of $6\,\sigma$. The ρ_{GL} of total chains is shown in Fig. 6c, where the GT&GF scheme exhibits a moderate grafting density of total chains. In short, choosing the GT&GF scheme seems wise because it provides a well-balanced density distribution and is more convenient in the synthesis process.

Despite this, there is an ongoing challenge associated with various crucial factors that significantly impact the one-pot GT&GF scheme. In this regard, we undertake a systematic and comprehensive examination of factors such as the reaction rate of the "grafting from" process, the initial total feeding ratio, and the step-addition operation. Our objective is to investigate the extent to which these factors impact the ultimate grafting density within the one-pot GT&GF scheme. Through this analysis, we aspire to chart a pathway towards effectively tuning nanoparticle composite materials in industrial settings.

We initiated our investigation by configuring a range of ligand chain grafting probabilities (P_r(A – T)) to systematically assess the influence of the GT reaction process across the three schemes (Fig. 7). This emphasis stems from the inherently slower motion of ligand chains compared to individual monomers. Prior to delving into this analysis, we introduced a parameter ξ, representing the ratio between the grafted density of ligand chains and that of grown chains. With an P_r(A – T), ξ initially rises before reaching a consistent plateau. Notably, in the region characterized by P_r(A – T) values up to 0.1 (Fig. 7), it becomes

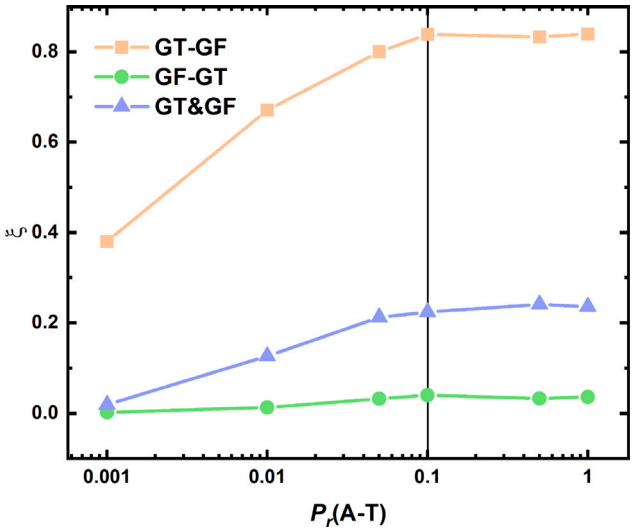

Fig. 7. The correlation between ξ and the chosen values of P_r(A – T) is investigated across three distinct schemes. Both the GT-GF and GF-GT strategies involve $5 \times 10^4\,\tau$ for each sub-process, while the GT&GF strategy is conducted for a singular $5 \times 10^4\,\tau$. The outcomes are based on data collected at the final reaction time.

evident that the reaction time is too brief to achieve the terminal plateau. In light of this insight, we designate a universally applicable value of P_r(A – T) = 0.5 for all GT reaction processes.

Theoretically, ξ exhibits higher trends in the GT-GF and GT&GF schemes compared to the GF-GT scheme, implying a greater grafting of ligand chains via GT reaction processes. However, the current research focus on ξ for the chains grown through the GF process. By evaluating ξ for these three schemes, we conclude that the GT&GF scheme maintains a lower ξ when comparing to GT-GF scheme. This trait positions the GT&GF scheme as an optimal choice for fabricating NP composite materials with two mixed polymer brushes, distinguished by chemical composition and properties. Importantly, the combination of the GT&GF scheme bears the potential for facile implementation in experimental settings.

As previously mentioned, we employ P_r(A – T) = 0.5 as a control condition (Fig. 8 RefG point), while focusing our subsequent investigation on the one-pot GT&GF scheme. Within this scheme, the reaction

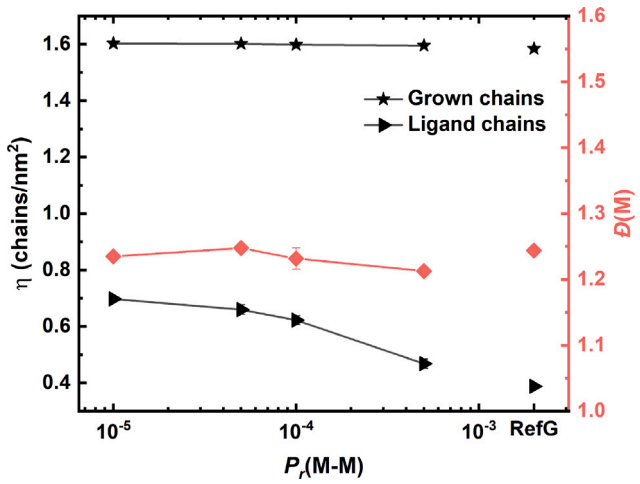

Fig. 8. The relationship between the grafting density and polydispersity of the selected values (P_r(M – M)) are examined within the GT&GF scheme.

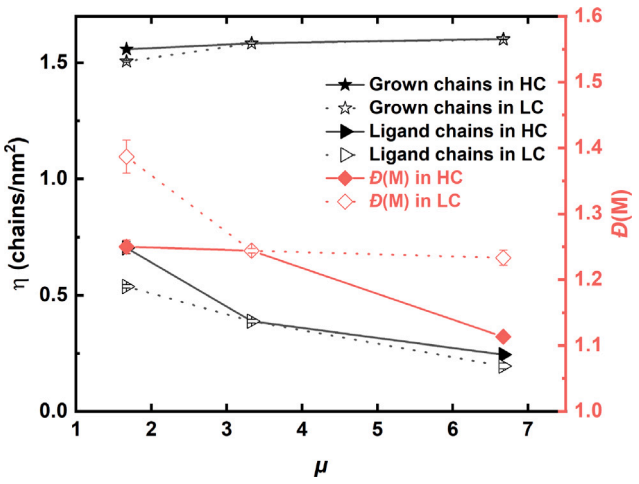

Fig. 9. The relationship between the grafted density (η) and the fraction (μ, representing the initial feeding ratios of monomers and ligand chains) at two different concentrations within the GT&GF scheme. The concentration in high concentration (HC) scenario is twice that of the low concentration (LC) scenario.

rate of monomers with initiator sites (P_r(M – M)) is crucial. It significantly influences the polymerization efficiency of the GF process, impacting the final fraction of grafted ligand chains by the GF process. Fig. 8 illustrates the profiles of grafting density (η) versus P_r(M – M). To determine P_r(M – M), we adopted the half/half method as proposed by Rosenbloom and colleagues [40]. For instance, a value of P_r(M – M) = 0.0005 was designated for the initial period of $5 \times 10^4\,\tau$, where the reaction between initiator sites (type B) and monomers (type M) varied as a function of selected P_r(M – M). Subsequently, during the latter period of $5\times10^4\,\tau$, the reaction was held at a fixed value of P_r(M – M) = 0.005 for each P_r(M – M). The trend depicted in Fig. 8 demonstrates that the grafted ligand chain content increases as P_r(M – M) decreases. This phenomenon signifies that when the value of P_r(M – M) during the initial period is low, the polymerization within the GF process is comparatively limited. Consequently, the ligand chains are more prone to graft via the GT process. Additionally, Fig. 8 highlights that the saturation level of grafted monomers in the GF process remains relatively constant. Crucially, the polydispersity index of Đ(M) maintains a low level of 1.20, indicative of effective grafting within the GF process. Overall, these findings confirm that a lower P_r(M – M) during the initial period enhances grafting performance for both the GT and GF processes.

For further inquiry, we delve into the influence of the initial total feeding ratio of monomers and ligand chains on the grafted content. In the low concentration (LC) scenario, we set the initial feeding ratios of monomers and ligand chains as μ = 1.67, 3.33, and 6.67 respectively, maintaining a constant count of 3840 ligand chains. In the high concentration (HC) scenario, although the same initial feeding ratios of μ are applied as in the low concentration case, we maintain a fixed number of 12 800 monomers while altering the number of ligand chains. Here, The concentration in the HC scenario is twice that in the LC scenario.

Illustrated in Fig. 9, both LC and HC scenarios exhibit relatively marginal changes in the number of grafted grown chains. However, in the LC context, despite a decrease in μ leading to a gradual increase in the grafting density (η) of grafted ligand chains (ranging from 0.19 to 0.54), the calculated polydispersity of Đ(M) shows a range from 1.23 to 1.40. Conversely, in HC case, as μ diminishes, the grafting density of grafted ligand chains sharply increase from 0.24 to 0.70. Remarkably, the polydispersity of Đ(M) remains around 1.20, indicative of a well-distributed incorporation of grafted grown chains. In this HC scenario, the grafted density of grown chains experiences a significant increase compared to the previously mentioned "changing of reaction rate P_r(M – M)" method. Simultaneously, the Đ(M) also stays at a low value (~1.24).

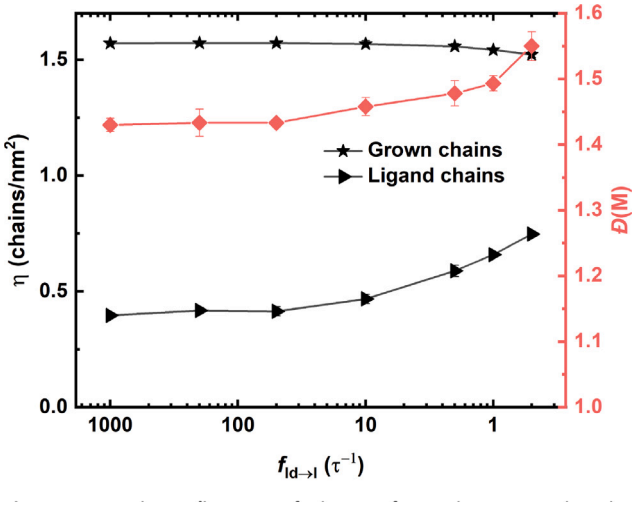

Fig. 10. The influence of the grafting density and polydispersity on the periodicity parameter within the GT&GF framework is investigated. The solid black line accompanied by squares corresponds to the quantification of surface-grafted monomers onto nanoparticles, while the black line featuring triangles corresponds to the quantification of surface-grafted ligand chains.

Recently, Rosenbloom et al. presented a concept concerning the controlled manipulation of polymer molecular mass distribution breadth and shape in RAFT polymerizations through the employment of chain transfer agents [40]. This notion provided valuable insights for our work. Similarly, in our previous study, we translated the step-addition approach from experimental practice to the simulation realm [41]. herein, we continue to explore the impact of altering the interval period of changing particle type within the GF process. Our inspiration comes from the concept of metered additions.

A cluster of 12,800 dormant beads (labeled as type Id) is randomly positioned outside the NPs within the simulation box. As the polymerization reaction commences, a permanent type transition is executed, whereby the dormant Id entities transform into active monomers (type M) for only one Id bead per period. To this end, we systematically implement a range of diverse changing periods, or says frequency ($f_{Id\to I}$), set as 1000, 200, 50, 10, 2, 1, and $0.5\,\tau^{-1}$, reflecting the idea

of metered additions. Subsequently, the monomers (type M) react with the initiator sites of type B on the NPs' surface.

As depicted in Fig. 10, the results indicate that the grafting density of ligand chains increases as the frequency $f_{\mathrm{Id}\to\mathrm{I}}$ decreases. This suggests a promising strategy for enhancing the incorporation of ligand chains. Notably, the grafting of grown chains tends to approach saturation during the GF process, maintaining a grafting density of approximately $1.55\,\mathrm{chains/nm^2}$ on each NP surface. At the initial stages of grafting, the mobility of individual monomers exceeds that of complete ligand chains, and monomers can swiftly reach the NPs' surface. In contrast, the grafting of ligand chains encounters significant challenges in approaching the NP surface, particularly during the concurrent monomer polymerization phase (GF process). This competitive scenario puts the GT process in a disadvantageous position.

As the frequency slow down (from 1000 to $0.5\,\tau^{-1}$), the influence of the GF process decreases significantly. This leads to a substantial increase in the grafting density of grafted ligand chains, rising from 0.40 to $0.75\,\mathrm{chains/nm^2}$. (black line with triangles in Fig. 10). Although this approach leads to an increased presence of grafted ligand chains on the NP surface, we observe an increased tendency of $Đ$(M) from its initial value of 1.45 to 1.55 (depicted by the red line in Fig. 10). Although this method does enhance the grafting density of ligand chains, it compromises the polydispersity of grown chains. Nevertheless, it is clear that this approach results in a significant increase in the grafting density of ligand chains.

4. Conclusions

In this paper, we use coarse-grained molecular dynamics (MD) simulations with stochastic reaction model to design a one-pot GT&GF strategy, which compared to two-step GT-GF and GF-GT. We find that this one-pot GT&GF strategy has a comparable polydispersity compared to a two-step process of the GF-GT strategy. Because of its one-pot synthesis method, it presents itself as a promising synthetic alternative, despite exhibiting a moderate grafting density in comparison to the GT-GF approach.

Given this, a series of factor, i.e., reaction rate of "grafting from", initial feeding ratio, step-addition operation, that will influence the final grafting density and polydispersity of this one-pot GT&GF strategy have been further detailed. It can be affirmed that a reduced value of the reaction rate of "grafting from" (P_r(M − M)) enhances the grafting conditions for both the GT and GF processes. For instance, reducing P_r(M − M) can lead to an increase in the density of grafted ligand chains while maintaining the density of grafted grown chains unchanged. Similarly, in terms of the initial feeding ratio, under high concentration conditions, reducing the value of μ also leads to an increased density of grafted ligand chains. Notably, both of these approaches maintain the $Đ$ of grown chains at lower values ($Đ$(M) = 1.24). Conversely, at lower concentrations, reducing μ leads to an increase in $Đ$(M) to 1.40, which might not be an optimal choice. Furthermore, the utilization of a step-addition operation, aimed at extending the addition frequency, while potentially leading to a substantial enhancement in the grafting density of ligand chains, is not advisable. This is due to its tendency to induce a pronounced increase in the polymer polydispersity index ($Đ$(M)) of grown chains. Generally, our work is desired to help for better uncovering the kinetics process during the preparation of bimodal polymer-anchored NPs by one-pot strategy and could give some of advices to rationally design and thus improve the performance of polymer-grafted NPs.

CRediT authorship contribution statement

Jinyuan Mao: Writing – original draft, Methodology, Investigation, Data curation, Conceptualization. **Jiajia Zhou:** Writing – review & editing, Supervision, Investigation, Conceptualization. **Hong Liu:** Writing – review & editing, Supervision, Project administration, Investigation, Conceptualization.

Declaration of competing interest

The authors declare that they have no known competing financial interests or personal relationships that could have appeared to influence the work reported in this paper.

Data availability

Data will be made available on request.

Acknowledgments

This work is supported by the National Natural Science Foundation of China (22273027, 22022303, 22373036). H.L. gratefully acknowledges the support from the Alexander von Humboldt Foundation, Germany. The computation of this work was made possible by the facilities of Information and Network Engineering and Research Center of SCUT.

References

[1] T.K. Patra, J.K. Singh, Coarse-grain molecular dynamics simulations of nanoparticle-polymer melt: Dispersion vs. agglomeration, J. Chem. Phys. 138 (14) (2013).
[2] L. Zheng, A.F. Xie, J.T. Lean, Polystyrene nanoparticles with anionically polymerized polybutadiene brushes, Macromolecules 37 (26) (2004) 9954–9962.
[3] M.R. Bockstaller, R.A. Mickiewicz, E.L. Thomas, Block copolymer nanocomposites: perspectives for tailored functional materials, Adv. Mater. 17 (11) (2005) 1331–1349.
[4] H. Wu, R. Ma, Y. Wang, X. Zhao, L. Zhang, Y. Gao, Manipulating the percolated network of nanorods in polymer matrix by adding non-conductive nanospheres: A molecular dynamics simulation, Compos. Sci. Technol. 229 (2022) 109694.
[5] S.K. Kumar, N. Jouault, B. Benicewicz, T. Neely, Nanocomposites with polymer grafted nanoparticles, Macromolecules 46 (9) (2013) 3199–3214.
[6] A. Jayaraman, Polymer grafted nanoparticles: Effect of chemical and physical heterogeneity in polymer grafts on particle assembly and dispersion, J. Polym. Sci. B: Polym. Phys. 51 (7) (2013) 524–534.
[7] V. Ganesan, A. Jayaraman, Theory and simulation studies of effective interactions, phase behavior and morphology in polymer nanocomposites, Soft Matter 10 (1) (2014) 13–38.
[8] D. Zhao, M. Di Nicola, M.M. Khani, J. Jestin, B.C. Benicewicz, S.K. Kumar, Self-assembly of monodisperse versus bidisperse polymer-grafted nanoparticles, ACS Macro Lett. 5 (7) (2016) 790–795.
[9] G. Munaò, A. De Nicola, F. Müller-Plathe, T. Kawakatsu, A. Kalogirou, G. Milano, Influence of polymer bidispersity on the effective particle–particle interactions in polymer nanocomposites, Macromolecules 52 (22) (2019) 8826–8839.
[10] L. Yu, N. Zhang, N.-N. Zhang, Q. Gu, Y. Xue, Y.-X. Wang, C.-L. Han, K. Liu, Z.-Y. Sun, H.-J. Qian, et al., Solvent-evaporation induced and mechanistic entropy-enthalpy-balance controlled polymer patch formation on nanoparticle surfaces, J. Phys. Chem. Lett. 12 (30) (2021) 7100–7105.
[11] S.R. Kutcherlapati, R. Koyilapu, U.M.R. Boddu, D. Datta, R.S. Perali, M.J. Swamy, T. Jana, Glycopolymer-grafted nanoparticles: synthesis using raft polymerization and binding study with lectin, Macromolecules 50 (18) (2017) 7309–7320.
[12] S.R. Kutcherlapati, R. Koyilapu, T. Jana, Poly (n-vinyl imidazole) grafted silica nanofillers: Synthesis by raft polymerization and nanocomposites with polybenzimidazole, J. Polym. Sci. A 56 (4) (2018) 365–375.
[13] M. Dhara, S. Rudra, N. Mukherjee, T. Jana, Hollow polymer nanocapsules with a ferrocenyl copolymer shell, Polym. Chem. 12 (27) (2021) 3976–3991.
[14] N. Mukherjee, A. Das, M. Dhara, T. Jana, Surface initiated raft polymerization to synthesize n-heterocyclic block copolymer grafted silica nanofillers for improving pem properties, Polymer 236 (2021) 124315.
[15] A. Das, N. Mukherjee, T. Jana, Polymer-grafted graphene oxide/polybenzimidazole nanocomposites for efficient proton-conducting membranes, ACS Appl. Nano Mater. 6 (7) (2023) 6365–6379.
[16] S. Rudra, M. Dhara, M. Chakraborty, T. Jana, Fluorinated polymer brush-grafted silica nanoparticles: Robust and durable self-cleaning coating materials, ACS Appl. Polym. Mater. 5 (9) (2023) 7443–7457.
[17] J. Song, P. Huang, X. Chen, Preparation of plasmonic vesicles from amphiphilic gold nanocrystals grafted with polymer brushes, Nat. Protoc. 11 (11) (2016) 2287–2299.
[18] L. Cheng, A. Liu, S. Peng, H. Duan, Responsive plasmonic assemblies of amphiphilic nanocrystals at oil-water interfaces, ACS Nano 4 (10) (2010) 6098–6104.
[19] L. Cheng, J. Song, J. Yin, H. Duan, Self-assembled plasmonic dimers of amphiphilic gold nanocrystals, J. Phys. Chem. Lett. 2 (17) (2011) 2258–2262.

[20] T.B. Martin, K.I.S. Mongcopa, R. Ashkar, P. Butler, R. Krishnamoorti, A. Jayaraman, Wetting–dewetting and dispersion–aggregation transitions are distinct for polymer grafted nanoparticles in chemically dissimilar polymer matrix, J. Am. Chem. Soc. 137 (33) (2015) 10624–10631.
[21] T.-Y. Tang, Y. Zhou, G. Arya, Interfacial assembly of tunable anisotropic nanoparticle architectures, ACS Nano 13 (4) (2019) 4111–4123.
[22] Y. Zhou, S.L. Bore, A.R. Tao, F. Paesani, G. Arya, Many-body potential for simulating the self-assembly of polymer-grafted nanoparticles in a polymer matrix, Npj Comput. Mater. 9 (1) (2023) 224.
[23] B. Natarajan, T. Neely, A. Rungta, B.C. Benicewicz, L.S. Schadler, Thermomechanical properties of bimodal brush modified nanoparticle composites, Macromolecules 46 (12) (2013) 4909–4918.
[24] T.B. Martin, P.M. Dodd, A. Jayaraman, Polydispersity for tuning the potential of mean force between polymer grafted nanoparticles in a polymer matrix, Phys. Rev. Lett. 110 (1) (2013) 018301.
[25] T.B. Martin, A. Jayaraman, Identifying the ideal characteristics of the grafted polymer chain length distribution for maximizing dispersion of polymer grafted nanoparticles in a polymer matrix, Macromolecules 46 (22) (2013) 9144–9150.
[26] R. Shi, H.-J. Qian, Z.-Y. Lu, Computer simulation study on the self-assembly of unimodal and bimodal polymer-grafted nanoparticles in a polymer melt, Phys. Chem. Chem. Phys. 19 (25) (2017) 16524–16532.
[27] C.-X. Li, J.-Y. Mao, S.-J. Li, Y. Wang, H. Liu, A long chain-induced depletion effect for abnormal grafting in the preparation of bimodal bidisperse polymer-grafted nanoparticles, Phys. Chem. Chem. Phys. 25 (7) (2023) 5627–5637.
[28] Y.-H. Xue, M.-W. He, X.-L. Liu, J.-Y. Xing, H. Liu, Preparation of nanoparticles grafted with bimodal-bidisperse polymers in nanocomposite, Compos. Sci. Technol. 197 (2020) 108250.
[29] A. Rungta, B. Natarajan, T. Neely, D. Dukes, L.S. Schadler, B.C. Benicewicz, Grafting bimodal polymer brushes on nanoparticles using controlled radical polymerization, Macromolecules 45 (23) (2012) 9303–9311.
[30] S. Minko, S. Patil, V. Datsyuk, F. Simon, K.-J. Eichhorn, M. Motornov, D. Usov, I. Tokarev, M. Stamm, Synthesis of adaptive polymer brushes via grafting to approach from melt, Langmuir 18 (1) (2002) 289–296.
[31] R.H. Hardin, N.J.A. Sloane, W.D. Smith, Tables of spherical codes with icosahedral symmetry, 1993, http://NeilSloane.com/icosahedral.codes/.
[32] M.P. Allen, D.J. Tildesley, Computer Simulation of Liquids, Oxford University Press, New York, 2017.
[33] Y. Zhu, H. Liu, Z. Li, H. Qian, G. Milano, Z. Lu, Galamost: Gpu-accelerated large-scale molecular simulation toolkit, J. Comput. Chem. 34 (25) (2013) 2197–2211.
[34] P.J. Flory, Thermodynamics of high polymer solutions, J. Chem. Phys. 10 (1) (1942) 51–61.
[35] J.A. Anderson, A. Travesset, Coarse-grained simulations of gels of nonionic multiblock copolymers with hydrophobic groups, Macromolecules 39 (15) (2006) 5143–5151.
[36] C. Pastorino, K. Binder, T. Kreer, M. Müller, Static and dynamic properties of the interface between a polymer brush and a melt of identical chains, J. Chem. Phys. 124 (6) (2006) 064902.
[37] H. Liu, M. Li, Z.-Y. Lu, Z.-G. Zhang, C.-C. Sun, Influence of surface-initiated polymerization rate and initiator density on the properties of polymer brushes, Macromolecules 42 (7) (2009) 2863–2872.
[38] H. Liu, H.-J. Qian, Y. Zhao, Z.-Y. Lu, Dissipative particle dynamics simulation study on the binary mixture phase separation coupled with polymerization, J. Chem. Phys. 127 (14) (2007).
[39] J. Midya, M. Rubinstein, S.K. Kumar, A. Nikoubashman, Structure of polymer-grafted nanoparticle melts, ACS Nano 14 (11) (2020) 15505–15516.
[40] S.I. Rosenbloom, R.J. Sifri, B.P. Fors, Achieving molecular weight distribution shape control and broad dispersities using raft polymerizations, Polym. Chem. 12 (34) (2021) 4910–4915.
[41] H. Liu, Y.-H. Xue, Y.-L. Zhu, F.-L. Gu, Z.-Y. Lu, Inverse design of molecular weight distribution in controlled polymerization via a one-pot reaction strategy, Macromolecules 53 (15) (2020) 6409–6419.